

# Synthesis and Electrochemical Properties of $0.7\text{LiMn}_{0.71}\text{Fe}_{0.29}\text{PO}_4 \cdot 0.3\text{Li}_3\text{V}_2(\text{PO}_4)_3/\text{C}$ Composite as High-Performance Cathode Materials for Lithium-Ion Batteries

XinYu Wang<sup>1</sup>, Zhi Su<sup>1,\*</sup>, ShanShan Li<sup>2</sup>

<sup>1</sup> College of Chemistry and Chemical Engineering, Xinjiang Normal University, Urumqi 830054, Xinjiang, China

<sup>2</sup> Bayingol Vocational and Technical College, Korla 841000, Xinjiang, China

\*E-mail: [suzhixj@sina.com](mailto:suzhixj@sina.com)

Received: 7 September 2016 / Accepted: 23 November 2016 / Published: 12 December 2016

---

A new polyanionic composite cathode materials,  $0.7\text{LiMn}_{0.71}\text{Fe}_{0.29}\text{PO}_4 \cdot 0.3\text{Li}_3\text{V}_2(\text{PO}_4)_3/\text{C}$ , was synthesized using a novel sol-gel method and with *N,N*-dimethyl formamide (DMF) as solvent. X-ray diffraction and transmission electron microscopy results indicated that the composite material was well-crystallized and a conductive carbon matrix surrounded the  $0.7\text{LiMn}_{0.71}\text{Fe}_{0.29}\text{PO}_4 \cdot 0.3\text{Li}_3\text{V}_2(\text{PO}_4)_3/\text{C}$  particles of grain size 20–50 nm. Elements Mn, V, and Fe in the composite were confirmed to be in +2, +3, and +2 valence states, respectively, by X-ray photoelectron spectroscopy. Electrochemical tests showed that as a cathode material,  $0.7\text{LiMn}_{0.71}\text{Fe}_{0.29}\text{PO}_4 \cdot 0.3\text{Li}_3\text{V}_2(\text{PO}_4)_3/\text{C}$  exhibited the best reversible capacities of 152.5, 130.1, 123.6, 109.5, and 83.6  $\text{mAh} \cdot \text{g}^{-1}$  at charge/discharge rates of 0.05, 0.1, 0.2, 0.5, and 1 C, respectively. It also retained  $147.2 \text{mAh} \cdot \text{g}^{-1}$  (91.8%) capacity in the Li-ion battery after 50 cycles at 0.05 C.

---

**Keywords:** lithium-ion cathode materials ; composite; sol-gel; nanoparticle; electrochemical properties

## 1. INTRODUCTION

Battery-powered electric vehicles produce no emission, they are environmentally friendly. Lithium ion batteries are considered to be the best option for electric vehicles due to their power density and high energy [1-3]. However, their inherently low ionic and electronic conductivities seriously limit the  $\text{Li}^+$  insertion/extraction and restrict their commercialization. Among these materials,  $\text{LiMnPO}_4/\text{C}$  (LMP/C) enjoys the advantages of high voltage (4.1 V), high volume energy density, but

the effect of Jahn-Teller lattice distortions of  $\text{Mn}^{3+}$  also leads to poor cycling stability. In order to overcome these problems of LMP/C, strategies such as carbon coating, ion doping, and compounding with other materials have been implemented [4-8].

One of these other materials is  $\text{LiFePO}_4/\text{C}$  (LFP/C). It has good electrical conductivity, and reports have indicated that it can improve the properties and cycle characteristics of other LMP/Cs. Ye et al. demonstrated an improved discharge capacity of  $149.2 \text{ mAh}\cdot\text{g}^{-1}$  at 0.1 C rate in  $\text{LiMn}_{0.9}\text{Fe}_{0.1}\text{PO}_4/\text{C}$  [9]. Liu et al. reported that  $\text{LiFePO}_4/\text{C}$  with size-controlled showed good rate performance, with an initial capacity of  $157.0 \text{ mAh}\cdot\text{g}^{-1}$  at 0.2 C [10]. Ma et al. synthesized Graphene- $\text{LiFePO}_4/\text{C}$  showed the initial charge/discharge capacity at 0.1 C is  $141 \text{ mAh}\cdot\text{g}^{-1}$  [11].

A third material,  $\text{Li}_3\text{V}_2(\text{PO}_4)_3/\text{C}$  (LVP/C), [12,13] shows a much higher  $\text{Li}^+$  migration rate owing to the open 3D framework of LVP. Encapsulation and composition with LVP [14-18] and V-doping [19] have been studied to improve the electrochemical performance of other LMP/Cs. Yang et al. prepared  $\text{LiFePO}_4\cdot\text{Li}_3\text{V}_2(\text{PO}_4)_3/\text{C}$  and found that the conductivity of LFP/C was greatly enhanced by the introduction of  $\text{Li}_3\text{V}_2(\text{PO}_4)_3/\text{C}$  [20]. Recently, Nevertheless, the exact effect and mechanism of LMP/C doping and/or compositing with dopants remain unknown.

Based on Our previous research [21-23], in this paper we design and synthesize the composite material  $0.7\text{LiMn}_{0.71}\text{Fe}_{0.29}\text{PO}_4\cdot 0.3\text{Li}_3\text{V}_2(\text{PO}_4)_3/\text{C}$  by a new sol-gel method that employed DMF as a solvent to control the particle size. The prepared composite was systematically compared to the single component LMP/C, and the binary composite  $\text{LiMn}_{0.71}\text{Fe}_{0.29}\text{PO}_4$  ( $0.71\text{LMP}\cdot 0.29\text{LFP}/\text{C}$ ) in terms of structure and electrical performance. As an electrode material, the  $0.7\text{LiMn}_{0.71}\text{Fe}_{0.29}\text{PO}_4\cdot 0.3\text{Li}_3\text{V}_2(\text{PO}_4)_3/\text{C}$  composite exhibited good electrochemical performance and high energy density.

## 2. EXPERIMENTAL

In this research all reagents were used directly without further depuration.

### 2.1 Synthesis

First,  $\text{V}_2\text{O}_5$  (0.55 g) was dissolved in 8 mL  $\text{H}_2\text{O}_2$  (30%), and glucose, the carbon source for carbonization were dissolved in 40 mL DMF. Then,  $\text{Mn}(\text{CH}_3\text{COO})_2\cdot 4\text{H}_2\text{O}$  (1.23 g),  $\text{Fe}(\text{CH}_3\text{COO})_2\cdot 4\text{H}_2\text{O}$  (0.49 g),  $\text{CH}_3\text{COOLi}\cdot 2\text{H}_2\text{O}$  (1.12 g), and  $\text{H}_3\text{PO}_4$  (85 wt.%) according to stoichiometric ratio were dissolved in 50 mL DMF. Then the two solutions were mixed and stirred to form a sol that was dried at  $80^\circ\text{C}$  for 8 h to obtain a gel. It was calcinated at  $700^\circ\text{C}$  for 12 h under Ar before cooling back to ambient condition. the  $0.7\text{LiMn}_{0.71}\text{Fe}_{0.29}\text{PO}_4\cdot 0.3\text{Li}_3\text{V}_2(\text{PO}_4)_3/\text{C}$  composite was obtain at last. The  $0.71\text{LMP}\cdot 0.29\text{LFP}/\text{C}$  and LMP/C materials were synthesized by the same way

## 2.2 Characterization

X-ray studies of the phase identities of the well-prepared samples were done on X-ray diffraction (Bruker D2) using Cu K $\alpha$  radiation at 30 kV and 10 mA. The crystal morphology was characterized by transmission electron microscopy (FEI Tecnai 20) at 200 kV. The valences of Fe, Mn and V in  $0.7\text{LiMn}_{0.71}\text{Fe}_{0.29}\text{PO}_4 \cdot 0.3\text{Li}_3\text{V}_2(\text{PO}_4)_3/\text{C}$  were determined by X-ray photoelectron spectroscopy (ESCALAB 250Xi).

## 2.3 Electrochemical Analysis

The electrochemical performance of materials were carried out by preparation into the coin-type half cells (LIR 2025) in glove box under Ar environmental protection. The cathode materials were composed of acetylene black, a poly (tetra • uoroethylene)binder, and a mixture of the synthesized materials in a 5 : 15 : 80 weight ratio. While lithium metal was used as reference electrodes, and the electrolyte was 1 M LiPF $_6$  dissolved in ethyl methyl ethylene carbonate, ethylene carbonate and dimethyl carbonate with a 1:1:1 volume ratio.

The charge and discharge experiments were conducted under ambient condition by using a battery test system LAND CT2001A (Wuhan, China) between 2.5 and 4.4 V. Cyclic voltammetry (CV) was made on LK2005A (China, Tianjin) electrochemical workstation in the potential ranges of 2.5–4.3 V at a scan rate of 0.1 mV·s $^{-1}$  under ambient condition. Electrochemical impedance spectroscopy (EIS) measurement was conducted by using Zahner IM6ex electrochemical workstation over a frequency from 10 Hz to 100 kHz with sinusoidal signal of 5 mV between the working and reference electrodes

## 3. RESULTS AND DISCUSSION

Fig. 1 displays the XRD patterns of three as-prepared composite samples. The  $\text{Li}_3\text{V}_2(\text{PO}_4)_3 \cdot \text{LiMn}_{0.67}\text{Fe}_{0.33}\text{PO}_4/\text{C}$  composite material consists of olivine structure  $\text{LiFe}_{0.5}\text{Mn}_{0.5}\text{PO}_4$  (PDF no. 42-580) and monoclinic formation  $\text{Li}_3\text{V}_2(\text{PO}_4)_3$  (PDF no. 47-0107). Due to the  $\text{LiMnPO}_4$  and  $\text{LiFePO}_4$  were homogeneous heterogeneous materials and formed a new solid solution with the same structure; thus, the solid solution and LVP did not generate a new compound, so no peaks corresponding to impurities were observed. The carbon contents in LMP/C,  $0.71\text{LMP} \cdot 0.29\text{LFP}/\text{C}$  and  $0.7\text{LiMn}_{0.71}\text{Fe}_{0.29}\text{PO}_4 \cdot 0.3\text{Li}_3\text{V}_2(\text{PO}_4)_3/\text{C}$  were 6.3, 7.1 and 6.8% as measured by elemental analysis.

The TEM and HRTEM images of the prepared materials are shown in Fig. 2. The  $\text{LiMnPO}_4/\text{C}$ ,  $\text{Li}_3\text{V}_2(\text{PO}_4)_3/\text{C}$ ,  $\cdot\text{LiMn}_{0.71}\text{Fe}_{0.29}\text{PO}_4/\text{C}$  and  $0.7\text{LiMn}_{0.71}\text{Fe}_{0.29}\text{PO}_4 \cdot 0.3\text{Li}_3\text{V}_2(\text{PO}_4)_3/\text{C}$  contained small particles of relatively uniform size (grain diameter: 20–50 nm) and all materials covered by about 2 nm carbon layer. The  $d$ -spacing 0.37 nm in Fig.2a is the LMP on the lattice planes (101), 0.36 nm in Fig.2b is the LVP on the lattice planes (130), the 0.33 and 0.37 nm in Fig.2c are representative the lattice planes (002) and (101) of solid solution  $\text{LiMn}_{0.71}\text{Fe}_{0.29}\text{PO}_4(\text{LMFP})$ , and the three  $d$ -spacing ,

0.43, 0.39 and 0.33 nm in Fig.2d are on the lattice planes (101), (120), and (131) of  $\text{LiFe}_{0.71}\text{Mn}_{0.29}\text{PO}_4$  and LVP in the composite  $0.7\text{LiMn}_{0.71}\text{Fe}_{0.29}\text{PO}_4 \cdot 0.3\text{Li}_3\text{V}_2(\text{PO}_4)_3$ , respectively. Therefore, the target material was verified as a composite of the  $\text{LiFe}_{0.67}\text{Mn}_{0.33}\text{PO}_4/\text{C}$  and the  $\text{Li}_3\text{V}_2(\text{PO}_4)_3/\text{C}$  [24]. And particles in all the samples were coated with a nanocarbon mesh, which served as a good electronic conduction network [25].

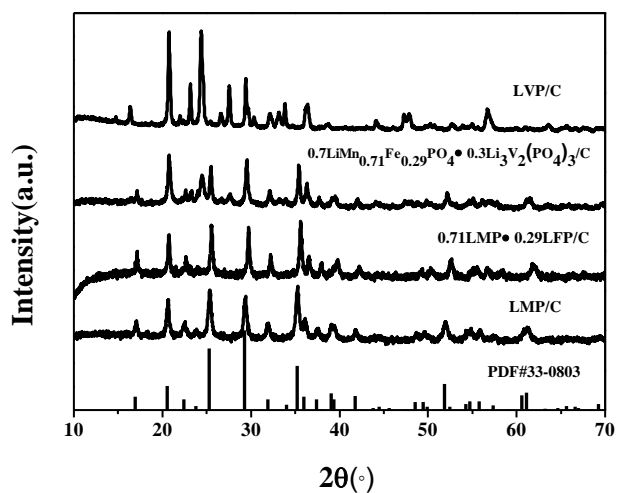


**Figure 1.** XRD patterns of the three samples ( $0.7\text{LiMn}_{0.71}\text{Fe}_{0.29}\text{PO}_4 \cdot 0.3\text{Li}_3\text{V}_2(\text{PO}_4)_3/\text{C}$ ,  $0.71\text{LMP} \cdot 0.29\text{LFP}/\text{C}$  and  $\text{LMP}/\text{C}$ .)

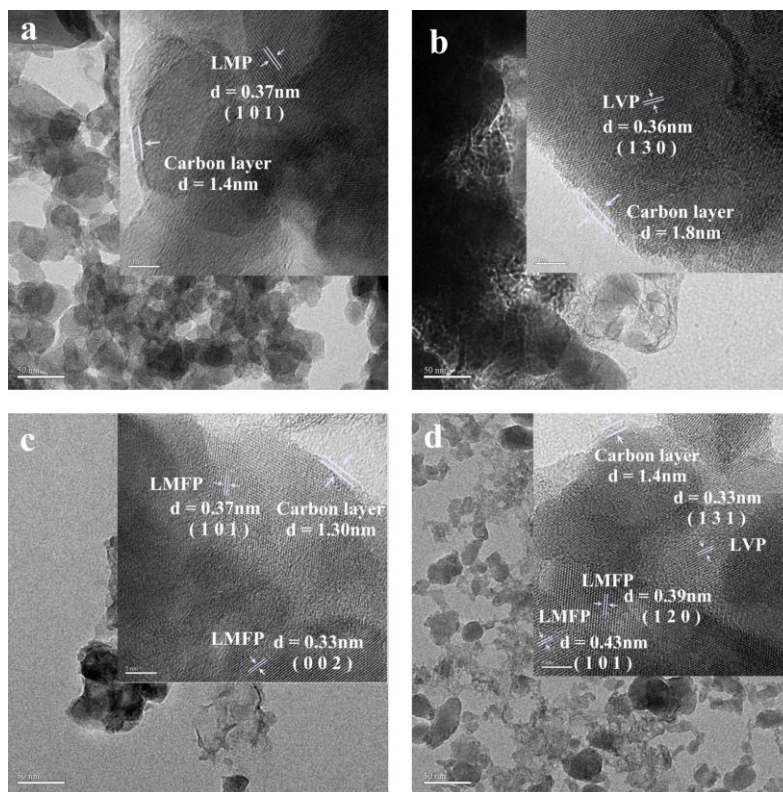
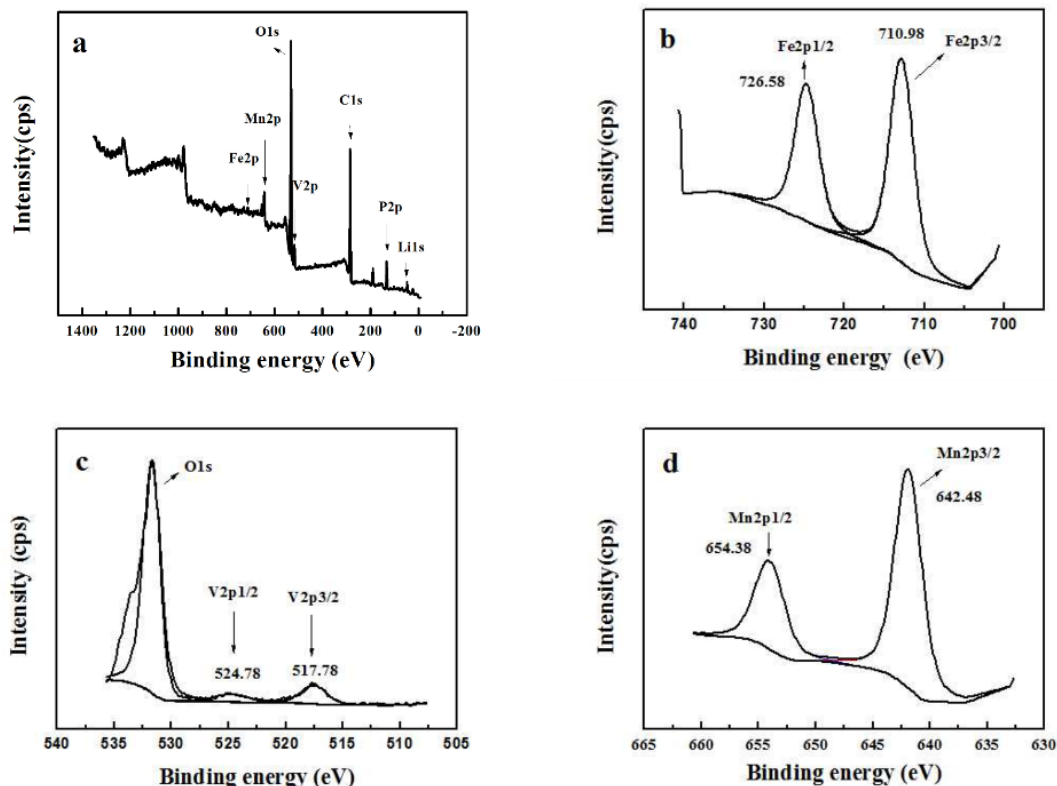


**Figure 2.** TEM and HRTEM images of (a)  $\text{LiMnPO}_4/\text{C}$ , (b)  $\text{Li}_3\text{V}_2(\text{PO}_4)_3/\text{C}$ , (c)  $\text{LiMn}_{0.71}\text{Fe}_{0.29}\text{PO}_4/\text{C}$  and (d)  $0.7\text{LiMn}_{0.71}\text{Fe}_{0.29}\text{PO}_4 \cdot 0.3\text{Li}_3\text{V}_2(\text{PO}_4)_3/\text{C}$

The valence states of V, Fe, and Mn in  $\text{Li}_3\text{V}_2(\text{PO}_4)_3 \cdot \text{LiMn}_{0.67}\text{Fe}_{0.33}\text{PO}_4/\text{C}$  are studied through XPS, with the wide-range spectra shown in Fig. 3a. The Li1s, P2p, and O1s binding energies are about 56.06, 134.94, and 532.06 eV, respectively, which are consistent with the literature values [26]. In Fig. 3b, 3c, and 3d, the spectra of Mn2p, V2p, and Fe2p each can be split into two peaks, implying that the valences of Mn, V, and Fe in the composites are +2, +3, and +2, respectively[27,28]. These results further indicate that LFP, LVP, and LMP coexist in the composite material.



7

**Figure 3.** Wide-range XPS spectra of  $0.7\text{LiMn}_{0.71}\text{Fe}_{0.29}\text{PO}_4 \cdot 0.3\text{Li}_3\text{V}_2(\text{PO}_4)_3/\text{C}$ , with separate energy regions corresponding to (b) Fe 2p, (c) V 2p, and (d) Mn 2p.

Fig. 4 initials the original charge/discharge profiles of all materials between 2.5–4.4 V. Not surprisingly, the discharge performance of LMP/C was poor ( $96.8 \text{ mAh} \cdot \text{g}^{-1}$ , curve a). In the  $0.7\text{LiMn}_{0.71}\text{Fe}_{0.29}\text{PO}_4 \cdot 0.3\text{Li}_3\text{V}_2(\text{PO}_4)_3/\text{C}$  composite (curve c), the discharge capacity increased to  $156 \text{ mAh} \cdot \text{g}^{-1}$ , likely due to the smaller particle size, which enlarges the reaction area and improves the utilization of the active material. The discharge performance of the  $0.7\text{LiMn}_{0.71}\text{Fe}_{0.29}\text{PO}_4 \cdot 0.3\text{Li}_3\text{V}_2(\text{PO}_4)_3/\text{C}$  composite is higher than the  $\text{LiMn}_{1/3}\text{Fe}_{1/3}\text{Co}_{1/3}\text{PO}_4/\text{C}$  composite in the study by Xiong et al [29]. Moreover the characteristic plateaus of LMP/C disappeared in  $0.7\text{LiMn}_{0.71}\text{Fe}_{0.29}\text{PO}_4 \cdot 0.3\text{Li}_3\text{V}_2(\text{PO}_4)_3/\text{C}$ , and a slow plateau at 3.5–4.0 V appeared due to the merger of plateaus from LVP/C and LMP/C.

The composite  $0.7\text{LiMn}_{0.71}\text{Fe}_{0.29}\text{PO}_4 \cdot 0.3\text{Li}_3\text{V}_2(\text{PO}_4)_3/\text{C}$  also demonstrated good cyclic stability after 50 cycles, as shown in Fig. 5a. This is probably due to Fe and V doping, that promoted the deintercalation of lithium ions from LMP. The discharge capacities of all sample materials at the first

and 50th cycles at the 0.05 C rate for are shown in Table 1. And the 0.7LiMn<sub>0.71</sub>Fe<sub>0.29</sub>PO<sub>4</sub>·0.3Li<sub>3</sub>V<sub>2</sub>(PO<sub>4</sub>)<sub>3</sub>/C composite material represented obvious improvements in the matter of the average voltage, energy retention rates and energy density.

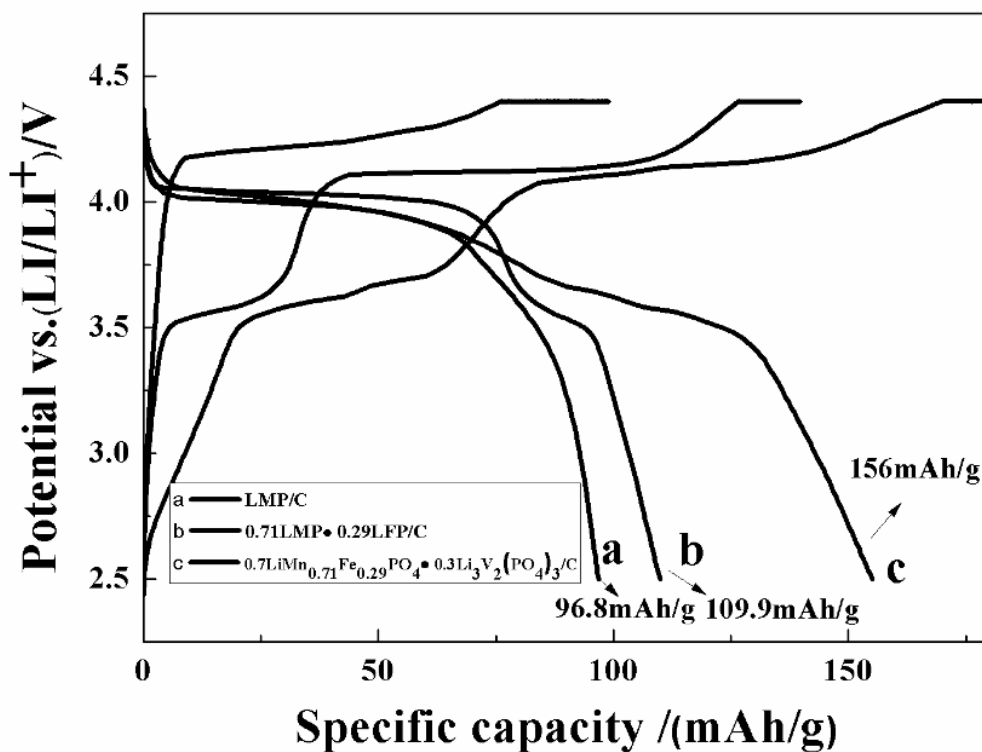


Figure 4. The first charge-discharge curves of all materials at 0.05 C.

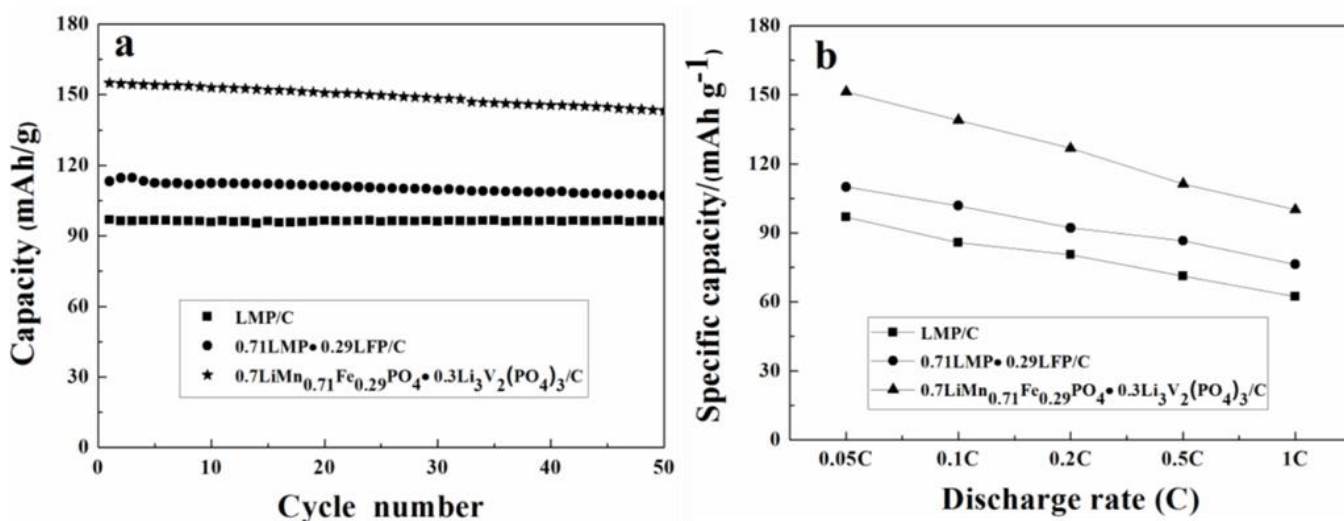


Figure 5. (a) Cycle performance of prepared composites tested under 0.05C (b) Rate capability of the prepared materials

Compared to the 0.95LiMn<sub>0.95</sub>Fe<sub>0.05</sub>PO<sub>4</sub>·0.05Li<sub>3</sub>V<sub>2</sub>(PO<sub>4</sub>)<sub>3</sub>/C composite material, the capacity retention rate of the 0.7LiMn<sub>0.71</sub>Fe<sub>0.29</sub>PO<sub>4</sub>·0.3Li<sub>3</sub>V<sub>2</sub>(PO<sub>4</sub>)<sub>3</sub>/C composite material is more excellent.[30]



It has the highest discharge energy density ( $537.28 \text{ W}\cdot\text{kg}^{-1}$  vs.  $360.79 \text{ W}\cdot\text{kg}^{-1}$  in LMP/C), and retention rate (95.6%) after 50 cycles. These results indicate that the  $0.7\text{LiMn}_{0.71}\text{Fe}_{0.29}\text{PO}_4\cdot 0.3\text{Li}_3\text{V}_2(\text{PO}_4)_3/\text{C}$  composite exhibits improved cycling stability. Fig. 5b shows the cycle performances of all sample materials at 0.05, 0.1, 0.5, and 1 C rates. Again, the cycle performance of  $0.7\text{LiMn}_{0.71}\text{Fe}_{0.29}\text{PO}_4\cdot 0.3\text{Li}_3\text{V}_2(\text{PO}_4)_3/\text{C}$  is much better than all other materials and at all the charge rates. At 1 C,  $0.7\text{LiMn}_{0.71}\text{Fe}_{0.29}\text{PO}_4\cdot 0.3\text{Li}_3\text{V}_2(\text{PO}_4)_3/\text{C}$  exhibited an excellent capacity of  $100 \text{ mAh}\cdot\text{g}^{-1}$ , whereas LMP/C showed only  $79.3 \text{ mAh}\cdot\text{g}^{-1}$ . In addition,  $0.7\text{LiMn}_{0.71}\text{Fe}_{0.29}\text{PO}_4\cdot 0.3\text{Li}_3\text{V}_2(\text{PO}_4)_3/\text{C}$  showed a lower polarisability than LMP/C, especially at high C-rates, thereby demonstrating improved electrochemical performance.

**Table 1.** Energy densities and discharge capacities of the materials, at first and 50th cycles.

Sample	Discharge capacity ( $\text{mAh}\cdot\text{g}^{-1}$ )			Average Voltage (V)		Discharge energy (W/kg)			The particle size (nm)
	1st	50th	C.R. (%) <sup>a</sup>	1st	50th	1st	50th	C.R. (%) <sup>b</sup>	
LMP/C	96.8	90.2	93.2	4.01	3.99	388.17	360.79	92.9	50-70
0.71LMP·0.29LFP/C	113.2	107.1	94.8	4.00	4.00	452.80	428.40	94.6	25-35
$0.7\text{LiMn}_{0.71}\text{Fe}_{0.29}\text{PO}_4\cdot 0.3\text{Li}_3\text{V}_2(\text{PO}_4)_3/\text{C}$	156.0	147.2	91.8	3.6	3.65	561.60	537.28	95.6	10-20

<sup>a</sup> C.R.: capacity retention ratios compared to the first cycle, <sup>b</sup> C.R.: energy retention ratios

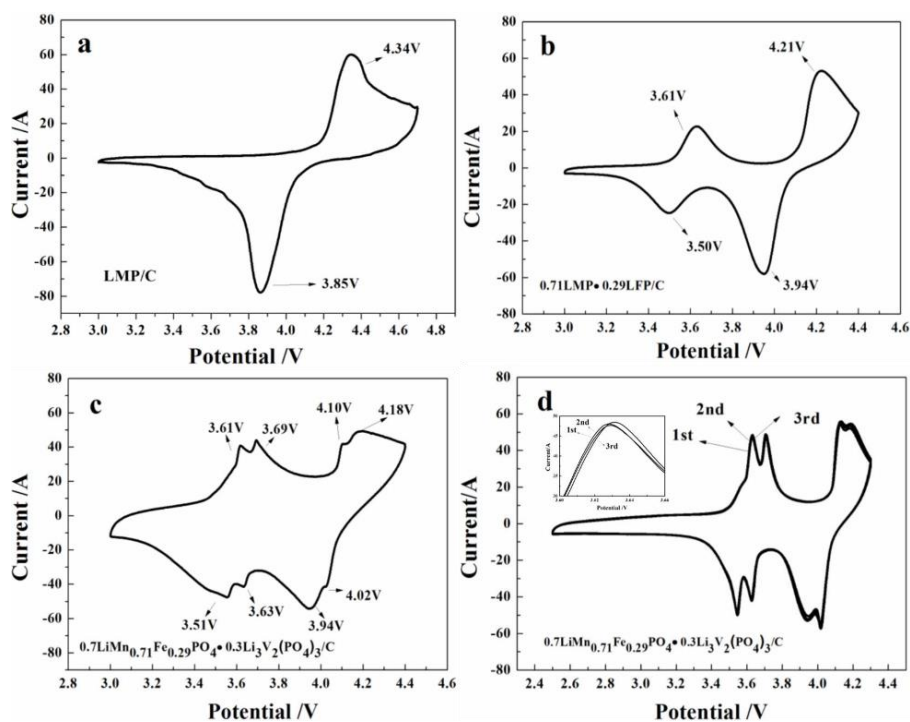


**Figure 6.** CV curves of (a) LMP/C, (b)  $0.71\text{LMP}\cdot 0.29\text{LFP}/\text{C}$  (c)  $0.7\text{LiMn}_{0.71}\text{Fe}_{0.29}\text{PO}_4\cdot 0.3\text{Li}_3\text{V}_2(\text{PO}_4)_3/\text{C}$ , and (d)  $0.7\text{LiMn}_{0.71}\text{Fe}_{0.29}\text{PO}_4\cdot 0.3\text{Li}_3\text{V}_2(\text{PO}_4)_3/\text{C}$  over three consecutive cycles

The CV curves of all materials electrodes are shown in Fig. 6a–c. For LMP/C (Fig. 6a), the redox potential peak at around 4.34/3.85 V, in accord with the oxidation of  $Mn^{2+}$  to  $Mn^{3+}$ .

The redox peaks of LMP/C and LFP/C were observed in 0.71 LMP·0.29LFP/C in Fig. 6b. The CV results of  $0.7LiMn_{0.71}Fe_{0.29}PO_4 \cdot 0.3Li_3V_2(PO_4)_3/C$  revealed four clear couples of redox peaks (Fig. 6c). The redox peaks at 3.61/3.51V, 3.69/3.63V and 4.10/4.02V tally with  $V^{4+}/V^{3+}$ , whereas the weak couple at 4.18/3.94 V is associated with LMP. Moreover, the redox peak of LFP was not discovered in the  $0.7LiMn_{0.71}Fe_{0.29}PO_4 \cdot 0.3Li_3V_2(PO_4)_3/C$  composite material, possibly due to its merger with the redox peak of LVP at 3.61/3.51V. These results are consistent with the corresponding charge/discharge curves. As shown in Fig. 7d, the curves of the three CV scan cycles almost overlap, indicating high electrochemical reversibility and low polarization. Therefore, CV analysis also confirmed that  $0.7LiMn_{0.71}Fe_{0.29}PO_4 \cdot 0.3Li_3V_2(PO_4)_3/C$  possesses great electrochemical properties.

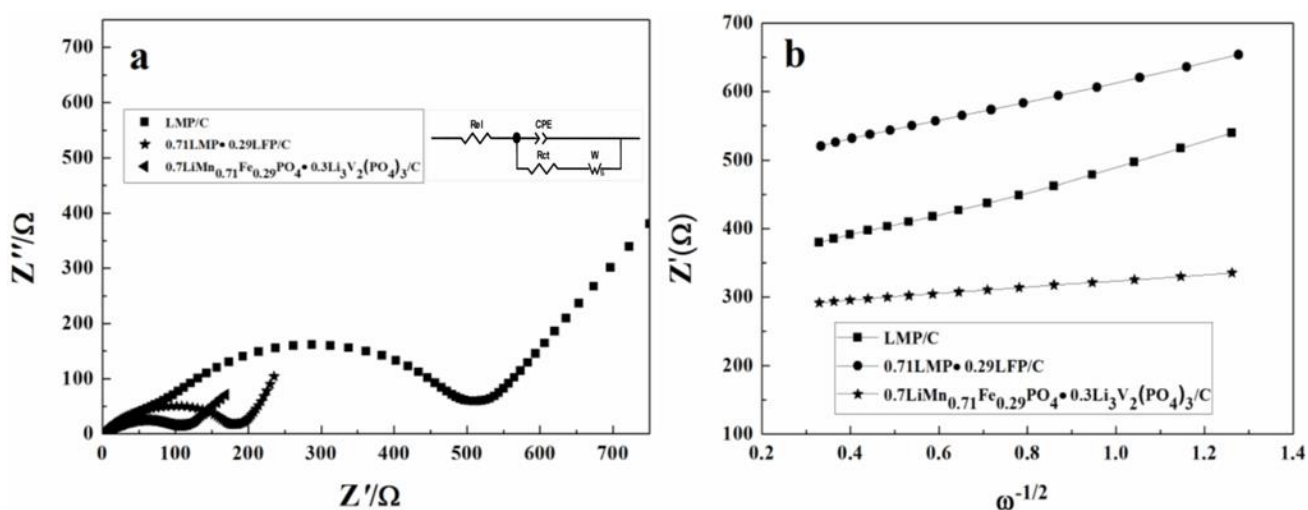


**Figure 7.** (a) Nyquist plots of all materials and (b) the relationship between  $Z'$  and  $\omega^{-1/2}$  for different compositions.

The Nyquist plots of three material electrodes are illustrated in Fig. 7a in the range of 10 Hz–100 kHz. The measurement was performed in the charged state of 4.1 V after an original cycling at 0.05 C. Fig. 8a shows that the Warburg impedance and charge transfer resistance of the  $0.7LiMn_{0.71}Fe_{0.29}PO_4 \cdot 0.3Li_3V_2(PO_4)_3/C$  material are much lower than those of LMP/C, indicating effectively improved Li extraction and insertion in the former. The parameters acquired by the equivalent circuit simulation of  $Li^+$  are listed in Table 2. In Fig. 7b, there is a linear relationship in the low-frequency region between  $Z'$  and the square root of frequency ( $\omega^{-1/2}$ ) in all the curves. The  $Li^+$  diffusion coefficient ( $D$ ) is calculated according to the following equation [31]

$$D = (0.5 R^2 T^2)/(A^2 n^4 F^4 C^2 \sigma^2) \quad (1)$$

where  $T$  represents the absolute temperature,  $R$  represents the gas constant,  $A$  represents the surface area of the electrode,  $F$  represents the Faraday constant,  $n$  represents the number of electrons lost per molecule during oxidization,  $C$  represents the molar concentration of  $Li^+$ , and  $\sigma$  represents the Warburg factor which is related to  $Z'$  by:

$$Z' = R_{el} + R_{ct} + \sigma \cdot \omega^{-1/2} \quad (2)$$



where  $R_{el}$  and  $R_{ct}$  are kinetic parameters independent of frequency,  $\omega$  represents the angular frequency in the low frequency region. According to equation (2),  $\sigma$  can be found as the slope in the plot of  $Z'$  vs  $\omega^{-1/2}$ . The diffusion coefficients calculated from equation (1) are listed in Table 3. For  $0.7\text{LiMn}_{0.71}\text{Fe}_{0.29}\text{PO}_4 \cdot 0.3\text{Li}_3\text{V}_2(\text{PO}_4)_3/\text{C}$ ,  $D = 2.00 \times 10^{-9} \text{ cm}^2 \cdot \text{s}^{-1}$ , almost six times that of LMP/C ( $3.00 \times 10^{-10} \text{ cm}^2 \cdot \text{s}^{-1}$ ). This result that the high performance of the  $0.7\text{LiMn}_{0.71}\text{Fe}_{0.29}\text{PO}_4 \cdot 0.3\text{Li}_3\text{V}_2(\text{PO}_4)_3/\text{C}$  composite is tally with seen in the battery performance tests.

**Table 2.** Electrochemical parameters from a.c. EIS results, calculated using Z-view software.

Sample	$R_{ct}$ ( $\Omega$ )	$W$ ( $\Omega$ )	CPE (F)	$D_{\text{Li}^+}$ ( $\text{cm}^2 \text{ s}^{-1}$ )
LMP/C	613.8	528.21	$9.06 \times 10^{-5}$	$3.00 \times 10^{-10}$
0.71LMP·0.29LFP/C	203.4	97.36	$6.45 \times 10^{-5}$	$2.67 \times 10^{-9}$
$0.7\text{LiMn}_{0.71}\text{Fe}_{0.29}\text{PO}_4 \cdot 0.3\text{Li}_3\text{V}_2(\text{PO}_4)_3/\text{C}$	392.4	239.32	$4.86 \times 10^{-5}$	$2.00 \times 10^{-9}$

Note:  $R_{ct}$  represents the charge-transfer resistance,  $W$  represents the Warburg impedance, and  $CPE$  represents the constant phase element.  $D_{\text{Li}^+}$  represents  $\text{Li}^+$  diffusion coefficient.

#### 4. CONCLUSIONS

The  $0.7\text{LiMn}_{0.71}\text{Fe}_{0.29}\text{PO}_4 \cdot 0.3\text{Li}_3\text{V}_2(\text{PO}_4)_3/\text{C}$  composite material with carbon conductive network,  $0.7\text{LiMn}_{0.71}\text{Fe}_{0.29}\text{PO}_4 \cdot 0.3\text{Li}_3\text{V}_2(\text{PO}_4)_3/\text{C}$ , was smoothly synthesized by a new sol-gel method, with a formulation designed to control the particle size. In Li-ion batteries, the composite material as the active cathode material showed excellent overall cycle stability, with discharge capacities of  $156.5 \text{ mAh} \cdot \text{g}^{-1}$  at 0.05 C and  $90.6 \text{ mAh} \cdot \text{g}^{-1}$  at 1 C. EIS and CV analysis results indicate that the composite material can efficiently facilitate Li insertion/extraction. In summary, the composite material  $0.7\text{LiMn}_{0.71}\text{Fe}_{0.29}\text{PO}_4 \cdot 0.3\text{Li}_3\text{V}_2(\text{PO}_4)_3/\text{C}$  combines the advantages of its three components (LFP/C, LMP/C, and LVP/C), thereby improving  $\text{Li}^+$  mobility compared to LMP/C and displaying good electrochemical performance.

#### ACKNOWLEDGEMENTS

This study was supported by the National Natural Science Foundation of China (No.21661030)

#### References

1. A.K. Padhi, K.S. Nanjundaswamy and J.B.D. Goodenough, *J Electrochem Soc.*, 144(1997) 1188.
2. J.M. Tarascon and M. Armand, *Nature.*, 414(2001) 359.
3. M.S. Whittingham, Y. Song, S. Lutta, P.Y. Zavalij and N.A.J. Chernova, *J Mater Chem.*, 15(2005) 3362.
4. S.Y. Chung, J.T. Bloking and Y.M. Chiang, *Nat Mater.*, 1(2002) 123.

5. P.S. Herle, B. Ellis, N. Coombs and L.F. Nazar, *Nat Mater.*, 3(2004) 147.
6. M. Yonemura, A. Yamada, Y. Takei, N. Sonoyama and R.J. Kanno, *J Electrochem Soc.*, 151(2004) A1352.
7. C. Delacourt, L. Laffont, R. Bouchet, C. Wurm, J.B. Leriche, M. *Chem Mater.*, 18(2006) 5520.
8. N. Meethong, H. Huang, S.A. Speakman, W.C. Carter and Y.M. Chiang, *Adv Funct Mater.*, 17(2007) 1115.
9. F. Ye, L. Wang, X. He, M. Fang, Z. Dai, *J Power Sources.*, 253(2014) 143.
10. Liu, J, Wang, Z, Zhang, G, Liu, Y, and Yu, A. *Int J Electrochem Sci.*, 8(2013)2378.
11. Ma, Y, Li, X, Sun, S, Hao, X, and Wu, Y. *Int. J. Electrochem. Sci.*, 8(2013)2842.
12. H. Liu, G. Yang, X. Zhang, P. Gao, L. Wang, J. Fang and X. Jiang, *J Mater Chem.*, 22(2012) 11039.
13. S.C. Yin, H. Grondey, P. Strobel, H. Huang and L.F. Nazar, *J Am Chem Soc.*, 125(2003) 326.
14. Y.C. Lin, G.T.K. Fey, P.J. Wu, J.K. Chang and H.M. Kao, *J Power Sources.*, 244(2013) 63.
15. F. Wang, J. Yang, Y. NuLi and J.Wang, *Electrochim Acta.*, 103(2013) 96.
16. K. Zaghib, M. Trudeau, A. Guerfi, J. Trottier, A. Mauger, R. Veillette and C.M. Julien, *J Power Sources.*, 204(2012) 177.
17. J. Wang, Z. Wang, X. Li, H. Guo, X. Wu, X. Zhang and W. Xiao, *J Alloy Compd.*, 581(2013) 836.
18. C.S. Yin, S.P. Strobel, H. Grondey and F.L. Nazar, *Chem Mater.*, 35(2004) 1456.
19. G. Yang, H. Ni, H. Liu, P. Gao, H. Ji, S. Roy and X.J. Jiang, *J Power Sources.*, 196(2011) 4747.
20. R.M. Yang, W. Ke and S. Wu, *J Power Sources.*, 165(2007) 646.
21. S. Li, Z. Su, X. Wang, *RSC Adv.*, 5(2015) 80170.
22. Y. Si, Z. Su, Y. Wang, T. Ma, J. Ding, *New J Chem.*, 39(2015) 8971.
23. S. Li, Z. Su, X. Jiang, A. Muslim, *Mater Lett.*, 154(2015) 29.
24. Y. Guo, Y. Huang, D. Jia, X. Wang, N. Sharma, Z. Guo and X. Tang, *J Power Sources.*, 246(2014) 912.
25. J. Mendialdua, R. Casanova and Y. Barbaux, *J Electron Spectrosc.*, 71(1995) 249.
26. Q. Chen, J. Wang, Z. Tang, W. He, H. Shao and J. Zhang, *Electrochim Acta.*, 52(2007) 5251.
27. S. Zhong, L. Wu and J. Liu, *Electrochim Acta.*, 74(2012) 8.
28. S.T. Myung, S. Komaba, N. Hirosaki, H. Yashiro and N. Kumagai, *Electrochim Acta.*, 49(2004) 4213.
29. Xiong, Y, Chen, Y, Zeng, D, Xiao, Q, Li, Z, and Lei, G.. *J Nanosci Nanotechno.*, 16(2016) 465.
30. L. Chen, B. Yan, H. Wang, X. Jiang and G. Yang, *J Power Sources.*, 287(2015) 316.
31. S. Liu, J. Xu, D. Li, Y. Hu, X. Liu and K. Xie, *J Power Sources.*, 232(2013) 258.